ChemPhotoChem

Research Article
doi.org/10.1002/cptc.202300201

Chemistry Europe
European Chemical Societies Publishing

www.chemphotochem.org

Solid-State Absorption, Luminescence, and Singlet Fission of Furanyl-Substituted Diketopyrrolopyrroles with Different π-Stacking Arrangements

Matouš Kratochvíl,[a] Muhammed A. Thottappali,[b] Stanislav Luňák, Jr.,[a] Karel Pauk,[c] David Rais,[b] Aneta Marková,[a] Jiří Pfleger,[b] Aleš Imramovský,*[c] and Martin Vala*[a]

Small modifications of the diketopyrrolopyrrole (DPP) molecular structure induced remarkable changes in its spectral and photophysical behavior. Using furan (F) heterosubstitution instead of thiophene (T) substituent resulted in a small blue shift and decreased Huang-Rhys factor of the absorption spectra in solution, irrespectively to *N,N'*-alkyls. Branching of alkyl side chains by formal 2-ethylation of *n*-hexyl substituent (C6 to EH) switched the slipped-stack arrangement, irrespectively on the heteroatoms. Consequent changes in steady-state absorption spectra of thin films were interpreted using time dependent density functional theory calculations, carried out on model dimers. Solid-state luminescence is weak and partially dependent on an excitation wavelength. Singlet fission was observed by femtosecond transient absorption spectroscopy, with considerably different yields for variously π-stacked FDPP-EH (30%) and FDPP-C6 (160%). The shape of triplet-triplet absorption spectra was also influenced by various π-stacking. The results are discussed in terms of different mixing of both Frenkel and charge transfer states in model dimers and different excitonic and electronic coupling in both types of π-stacks, visualized by natural transition orbitals.

Introduction

Singlet fission (SF) is an example of a multiexciton generation process, in which the singlet state splits into two triplet states.[1] Although the research of SF is motivated mainly by its possible impact on increasing photovoltaic efficiency,[2] some other applications are also considered.[3] SF can proceed either in an intra- or inter-molecular way and requires exoergicity, i.e. the lowest triplet state should be about half or less of the energy of the lowest singlet state. Typical examples of molecules that fulfill this condition are some acenes, dyes (ryleneimides, diketopyrrolopyrroles, and carotenes), polymers, and various diradicaloids.[4] Except for energetics, the distance and mutual orientation of the chromophores play a crucial role in the SF efficiency.[5] Interchromophoric coupling parameters can be tuned either by a connecting unit in covalently bound oligomers undergoing intramolecular SF,[6] or by crystal engineering in solids, where intermolecular SF takes place.[7] Covalently linked diketopyrrolopyrroles (DPPs) show an intramolecular SF only rarely,[8] as they usually undergo different nonradiative deactivation, like charge separation.[9] On the other hand, intermolecular SF always takes place in thiophene (T) disubstituted DPPs with various *N,N'*dialkyls (TDPPs in Scheme 1, Figure 1) in a solid state.[10] SF of DPP furanyl heteroanalogues (FDPPs in Scheme 1) was never studied, although the theoretical calculations predict their suitable energetics on a molecular level,[11] confirmed partially by triplet fusion experiments.[12]

Light absorption in molecular aggregates results in the generation of singlet excitons.[13] These aggregates can be classified as J (H), according to negative (positive) excitonic (Coulombic, dipole-dipole) coupling, i.e. according to the bright (dark) character of the lowest Frenkel (FE) state.[14] Charge

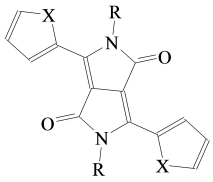

X = O, R = n-hexyl	**FDPP-C6**
X = S, R = n-hexyl	**TDPP-C6**
X = O, R = 2-ethyl-hexyl	**FDPP-EH**
X = S, R = 2-ethyl-hexyl	**TDPP-EH**

Scheme 1. Compounds under study.

[a] *Dr. M. Kratochvíl,[+] Dr. S. Luňák, Jr., A. Marková, Prof. M. Vala*
Materials Research Centre, Faculty of Chemistry
Brno University of Technology
Purkyňova 464/118, 61200 Brno (Czech Republic)
E-mail: vala@fch.vut.cz

[b] *M. A. Thottappali,[+] Dr. D. Rais, Dr. J. Pfleger*
Department of Polymers for Electronics and Photonics, Institute of Macromolecular Chemistry
Czech Academy of Sciences
Heyrovského nám. 2, 16206 Prague 6 (Czech Republic)

[c] *Dr. K. Pauk, Prof. A. Imramovský*
Institute of Organic Chemistry and Technology, Faculty of Chemical Technology
University of Pardubice
Studentská 95, 53009 Pardubice (Czech Republic)
E-mail: Ales.Imramovsky@upce.cz

[+] *equal contribution*

Supporting information for this article is available on the WWW under https://doi.org/10.1002/cptc.202300201

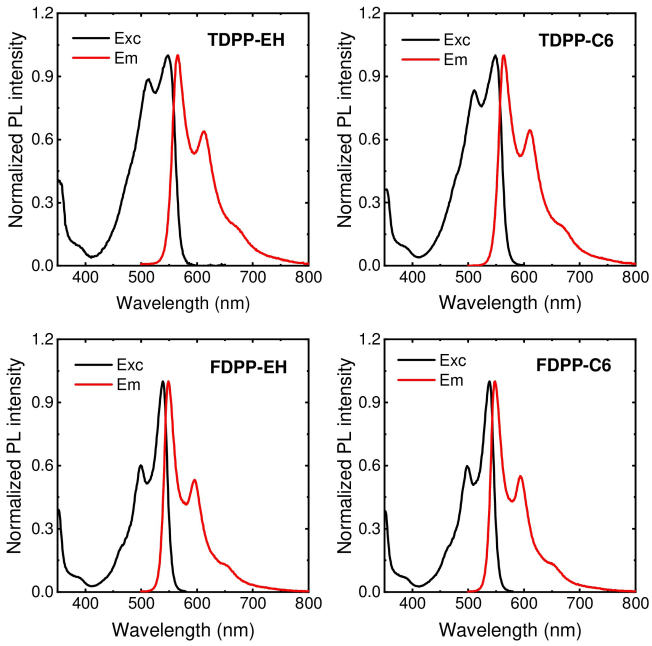

Figure 1. Fluorescence excitation (black lines) and emission spectra (red lines) in chloroform. **TDPP-EH** λ_{Exc} 612 nm, λ_{Em} 340 nm; **TDPP-C6** λ_{Exc} 611 nm, λ_{Em} 339 nm; **FDPP-EH** λ_{Exc} 597 nm, λ_{Em} 340 nm; **FDPP-C6** λ_{Exc} 593 nm, λ_{Em} 340 nm.

transfer (CT) states can arise if the long-range Coulombic interaction is accompanied by short-range coupling between the molecules with a wave function overlap.[14b] Generally, the vibronic structure of the solid-state absorption (SSA) bands of conjugated molecules, described by a ratio of the intensities of 0–1 and 0–0 bands R_{ABS},[14c] is modulated by the vinylene/ring stretching progressions and depends on the Huang-Rhys factor S of an isolated molecule and the strength of the excitonic coupling. The short-range interaction may give rise to a separate CT band in SSA, which is, however, often overlaid by the vibronic progression of the more intense bright FE band and may cause a red shift of the FE band even for H-aggregates. Thus H-aggregates are unambiguously defined by the higher energy of the bright (carrying the oscillator strength) FE excited state with respect to the dark one, regardless of whether the transition energy of the aggregate bright state lies above or below the transition energy of the monomer.[14d] Singlet exciton can be converted to the correlated triplet pair with overall singlet multiplicity either directly or by an indirect mechanism, mediated by the CT state.[15] Although J-type aggregation should be theoretically preferred for SF, H-aggregates are also able to show very efficient SF near the upper 200% limit.[16]

TDPPs molecules crystallize in a limited number of usually H-type slipped-stacked arrangements, forming crystal columns with an energy splitting of FE and CT states, which considerably depends on the mutual translation between neighbour molecules that can be efficiently influenced by β-branching of *N*,*N*'dialkyls.[17] Consequently, markedly different R_{ABS} were found for **TDPP-EH**, as compared to **TDPP-C6**.[10b] Furthermore, the broad SSA spectral bands were found to be composed of two electronic transitions with an energy separation dependent on the side alkyl branching.[18] On the other hand, only medium SF efficiency was found in both cases, 110% and 70% for **TDPP-C6** and **TDPP-EH** respectively.[10b] A similar value (120%) for **TDPP-C6** was also found later.[10d] On the other hand, the early report on the almost absolute SF efficiency found for *N*,*N*'-dimethyl TDPP[10b] was later down corrected.[10e] **FDPP-C6**[19] shows the same type of slipped stacked arrangement, but with a smaller plane-to-plane (PP) distance and higher molecular rigidity with respect to the heteroaryl torsion,[17] compared to **TDPP-C6**.[10b] X-ray diffraction (XRD) of the crystalline **TDPP-EH**[20] suggests even a longer PP distance compared to **TDPP-C6**, while the packing arrangement of **FDPP-EH** is unknown.

The smaller the Huang-Rhys factor S of an isolated molecule, the lower the torsional flexibility of terminal (hetero)aryls.[21] Since FDPPs are generally more rigid than TDPPs, we have synthesized a set of four π-isoelectronic DPP derivatives (Figure 1) to tune independently both parameters that influence the shape of the SSA bands, i.e. molecular Huang-Rhys factor by S→O formal heterosubstitution, and intermolecular excitonic coupling, driven by different molecular stacking that depends on the alkyl branching. More distinct spectral features in the SSA spectra of FDPPs allowed us to determine the energies of FE and CT states and the bandwidth. Furthermore, SF efficiency could be established more precisely, and relatively good quality SF invoked triplet-triplet absorption (TTA) spectra were extracted from transient absorption spectra and interpreted in terms of their dependence on molecular stacking.

Results and Discussion

The spectral and photophysical properties were measured in chloroform (Table 1, Figure 1). FDPPs show a very small but still detectable hypsochromic shift (~0.04 eV) with respect to TDPPs, a smaller Stokes shift (< 0.04 eV) than TDPPs (~0.06 eV) and a similar distance between 0–0 and 0–1 vibronic bands related to vinylene stretching (0.18–0.19 eV in the excitation spectrum) and similar fluorescence quantum yields (PLQY) and lifetimes. The Huang-Rhys factor S obtained from the emission spectra is generally lower than in excitation (Figure 1), indicating higher rigidity of the emitting state. Comparing the Huang-Rhys factors obtained from the excitation spectra, we found it considerably lower for FDPPs (~0.60) than for TDPPs (over 0.80), confirming the expected higher torsional flexibility of the latter in the ground state.[19,21]

Table 1. Optical properties of DPP derivatives in chloroform. The main peaks are marked in bold.

Compound	λ_{max} (nm)			PLQY (%)	τ_F (ns)
	Absorbance	Excitation	Emission		
FDPP-C6	499; **539**	498; **539**	548; **593**	85 ± 2	5.87
FDPP-EH	500; **540**	500; **540**	549; **597**	91 ± 3	5.93
TDPP-C6	513; **550**	511; **550**	564; **611**	79 ± 5	6.00
TDPP-EH	514; **547**	514; **548**	565; **612**	90 ± 4	5.96

SSA spectra of the vacuum evaporated films do not show such resolved vibronic bands as in the solution (Figure 2), but they are sufficiently resolved for an analysis of the impact of the excitonic coupling on $R_{ABS} = I_{0-1}/I_{0-0}$ (Table 2). The qualitative analysis shows at least three important spectral features. First, all compounds show a bathochromic shift of absorption maxima as compared to the maxima in solution. This shift is remarkable for C6 substituted derivatives (0.23 and 0.19 eV), while for EH derivatives it is considerably smaller (0.03 and 0.07 eV). Second, the R_{ABS} ratio is always higher than the corresponding Huang-Rhys factor S in solution absorption. Their mutual ratio R_{ABS}/S is 1.15 and 1.25 for **FDPP-C6** and **TDPP-C6**, respectively, and bigger for **FDPP-EH** (1.81) and **TDPP-EH** (3.19). Third, the local absorption maximum of **FDPP-C6** at 2.59 eV is 0.52 eV blue shifted with respect to 0–0 maximum. This shift is out of the usual vinylene stretching vibronic patterns, modified by excitonic coupling.[14] This distinct spectral feature is missing in the SSA spectrum of **TDPP-C6**. According to the theory,[14] all four compounds should be in H-aggregates, due to $R_{ABS} > S$. Considerably lower R_{ABS} of C6 with respect to the corresponding EH derivatives with almost the same S, indicates a smaller excitonic coupling. The higher bathochromic shift for C6 derivatives in the solid state should be a result of destructive interference of long-range Coulombic and short-range electronic coupling.[22] The irregular band in the SSA spectrum of FDPP-C6 is considered a candidate for the CT transition.

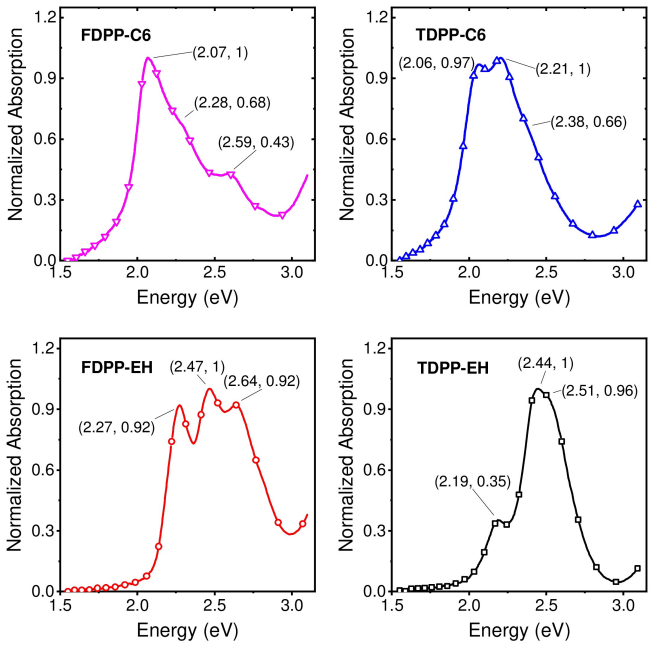

Figure 2. Absorption spectra of thin films prepared by vacuum vapor deposition.

Table 2. R_{ABS} and energy of 0–0 transition in the solid state absorption and emission spectra.

Compound	Absorption		Emission
	E_{00} [eV]	R_{ABS}	E_{00} [eV]
FDPP-C6	2.07	0.68	1.92
FDPP-EH	2.27	1.09	2.11
TDPP-C6	2.06	1.03	
TDPP-EH	2.19	2.84	

Solid state emission (SSE) of both FDPPs (Figure 3, Table 2) is generally weak (PLQY less than 0.01, as for TDPPs reported earlier[10a,d]), and, hence, it does not form an important deactivation channel after excitation. Both emissions show similar Stokes shift (0.15 eV with respect to the absorption, 0.14 eV with respect to the excitation maxima), considerably higher as compared to Stokes shift in solution. Both emission spectra of FDPPs (especially of **FDPP-C6**) are considerably more blurred than in solution, so the excitation ones. The excitation spectra of both FDPPs show differences with respect to SSA. The short wavelength area below the 0–2 progression of the excitation spectrum is enhanced with respect to the 0–0 peak in **FDPP-C6**, as compared to SSA, while in **FDPP-EH** the area around 0–1 progression is partially reduced relative to the intensity of 0–0 band. Both these observations mean that (contrary to the solution) the minor radiative relaxation process does not follow Kasha's rule. No dependence on excitation wavelength was observed for the major process, i.e. singlet fission (*vide infra*).

A simple quantum chemical (QCH) modelling based on density functional theory (DFT) was carried out to understand the details of the SSA and SSE spectra of FDPPs. A set of six slipped π- stacked dimers, characterized by center-to-center (CC) and plane-to-plane (PP) distances, was found using dimer optimization of non-alkylated model **FDPP-H** with M06-2X xc functional (Figure S1), as in the previous report on TDPPs.[17] The dimer optimization at ωB97X-D/6-31G(d,p) level gives only dimers **1**–**4** (Table S1). The geometries (Figure 4) of the most stable dimers **3** (found experimentally for both **TDPP-C6**[10b] and **FDPP-C6**[19]) and **4** (found for **TDPP-EH**[10b] and assumed to be present also in **FDPP-EH**), computed with ωB97X-D xc functional, were chosen for excited state calculations using time dependent (TD) DFT, as they give more realistic PP distances (Table S1). The characteristics of computed adiabatic excited states of these model dimers, computed with proven[23–24] ωB97X-D xc functional, are presented in Table 3. As the absolute values of computed excitation energies of **FDPP-H** are about 0.6–0.7 eV higher than measured 0–0 maxima of both alkylated

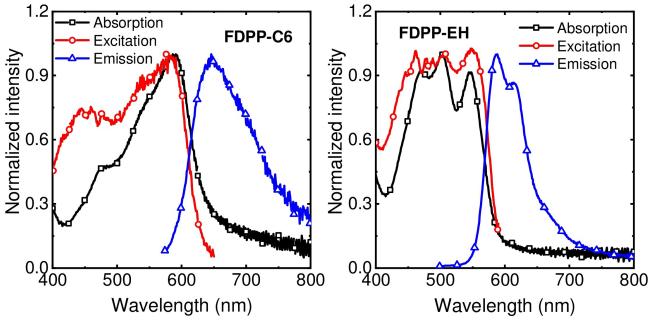

Figure 3. Absorption, emission, and excitation luminescence spectra of FDPP derivatives thin films. **FDPP-C6** λ_{Exc} 700 nm, λ_{Em} 540 nm; **FDPP-EH** λ_{Exc} 612 nm, λ_{Em} 477 nm.

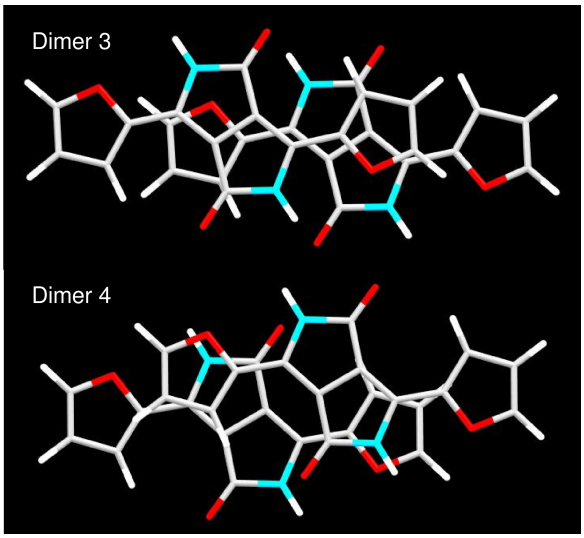

Figure 4. DFT (ωB97X-D/6-31G(d,p)) optimized dimer **3** (CC = 4.656 Å, PP = 3.171 Å) and **4** (CC = 4.510 Å, PP = 3.263 Å) of model **FDPP-H**.

Table 3. TD DFT (ωB97X-D/6-31 + G(d,p)) computed excitation energies on optimized geometries of the dimers composed of model **FDPP-H** molecules from Figure 4. S_1 state of a monomer was located at 2.849 eV with $f_{osc} = 0.591$ at the same computational level. E_{exc} = excitation energy, f_{osc} = oscillator strength.

Dimer	State	E_{exc} [eV]	f_{osc}	Orbital configuration
3	$1A_g$	2.672	0	H−1→L
	$1A_u$	2.738	0.793	H→L
	$2A_g$	3.146	0	H→L + 1
	$2A_u$	3.290	0.223	H−1→L + 1
4	$1A_g$	2.559	0	H→L
	$1A_u$	2.918	0.817	H→L + 1
	$2A_g$	3.144	0.157	H−1→L
	$2A_u$	3.181	0	H−1→L + 1

FDPPs (Table 2), the difference values (Table 4) were computed according to previously reported methodology.[17] Two directly comparable energy differences give remarkable agreement between theory and experiment. First, the energy difference between 0–0 maxima for **FDPP-C6** and **FDPP-EH** (Table 2) is 0.20 eV, while the difference between $1A_u$ states of dimers **3** and **4** of model **FDPP-H** is 0.18 eV. Second, the energy difference between 0–0 maximum and irregular peak in SSA of **FDPP-C6** is about 0.52 eV, while the difference between the $1A_u$ and $2A_u$ states in the dimer **3** of **FDPP-H** is 0.55 eV (Table 4). The computed E_{CF} values 0.23 eV and 0.55 eV (Table 4) relate also well to the values obtained for TDPPs with either linear (0.47–0.49 eV) or β-branched (0.23 eV) alkyl chains.[18] The absence of a distinct spectral feature, relating to a transition to CT state for **TDPP-C6** (PP = 3.408 Å), with the same type of slipped stack arrangement as **FDPP-C6** (PP = 3.296 Å), is ascribed to the shorter plane-to-plane distance from XRD for the latter.[17] The considerably bigger E_{EC} values for the slipped stacked dimer **4** lead to a long wavelength tail in SSA, i.e. to the difference between the shape of the absorption edge below 0–0 peak for **FDPP-EH** and **TDPP-EH**, as compared to **FDPP-C6** and **TDPP-C6** (Figure 2). As expected,[14a] higher E_{EC} of the dimer **4**, compared to dimer **3**, also causes a considerable increase of R_{ABS} (Figure 2, Table 2), when going from **FDPP-C6** to **FDPP-EH**. Thus, we consider the slipped stacked arrangement of **FDPP-EH** in dimer **4**-like configuration as confirmed and the **FDPP-H** model as giving relevant results on a semiquantitative level for further discussion. According to H/J assignment, **FDPP-C6** is a weak red-shifted H-aggregate, while **FDPP-EH** is a strong blue-shifted H-aggregate. We note only, that the geometrical calculation gives a bit lower PP values, than the experimental ones. We can only speculate by analogy with TDPPs,[17] that PP for β-branched **FDPP-EH** will be considerably higher than for **FDPP-C6**, i.e. around 3.5 Å.

Table 4. The excitation energy difference between monomer and dimer $E_{DM} = E_{exc}$(monomer, $1A_u$) − E_{exc}(dimer, $1A_u$), excitonic coupling $E_{EC} = 1/2$ (E_{exc}(dimer, $1A_g$) − E_{exc}(dimer, $1A_u$)), energy splitting between allowed CT and FE state $E_{CF} = E_{exc}$(dimer, $2A_u$) − E_{exc}(dimer, $1A_u$) and the ratio of their intensities $R_{FC} = f_{osc}$(dimer, $1A_u$)/f_{osc}(dimer, $2A_u$) of model **FDPP-H** molecules from Figure 4. Negative value of E_{EC} means J-aggregate, positive H-aggregate. E_{exc} and f_{osc} were taken from Table 3.

Dimer	E_{DM} [eV]	$2 \cdot E_{EC}$ [eV]	E_{CF} [eV]	R_{FC}
3	+0.111	−0.066	0.552	3.56
4	−0.069	−0.359	0.226	5.20

Generally, TD DFT computed excited states are adiabatic. So, the assignment of $1A_u$ and $2A_u$ states to the allowed FE and CT states, respectively, describes only their prevailing character arising from the FE/FE long-range and FE/CT short-range mixing of pure diabatic states. Strong FE/FE mixing thus dominates **FDPP-EH** in the dimer **4** arrangement, with an E_{EC} value more than five times higher than for dimer **3** of **FDPP-C6**. On the other hand, more than twice the higher value of E_{CF} for **FDPP-C6** slip-stacked in dimer **3** fashion signalizes considerably higher FE/CT mixing and thus more pronounced participation of CT character in the lowest bright excited state.[25] From the symmetry point of view the allowed FE and CT transitions of both FDPPs are of $a_u \rightarrow a_g$ and $a_g \rightarrow a_u$ character, respectively. There is a considerable difference between these transitions, with respect to the changes of the electron density in the area between the molecules, as visualized by corresponding natural transition orbitals (NTOs) in Figure 5. As expected from the lower E_{CF} value for **FDPP-EH** both allowed states show a relatively pure FE (Figure 5c) and CT (Figure 5d) character without the significant changes of electron density between the monomers. On the other hand, the intermolecular density is considerably changed during the excitation to both allowed states of **FDPP-C6** in a mutually opposite way. It is increased for transition 2 (Figure 5a) and decreased for transition 4 (Figure 5b). Such a dramatic change in electron density distribution, accompanying the transition, causes more efficient electron-phonon coupling with intermolecular vibrations and consequently the main spectral bands in both SSA and SSE are more blurred, as compared to **FDPP-EH**, where the transition to pure FE state shows less significant intermolecular vibrational

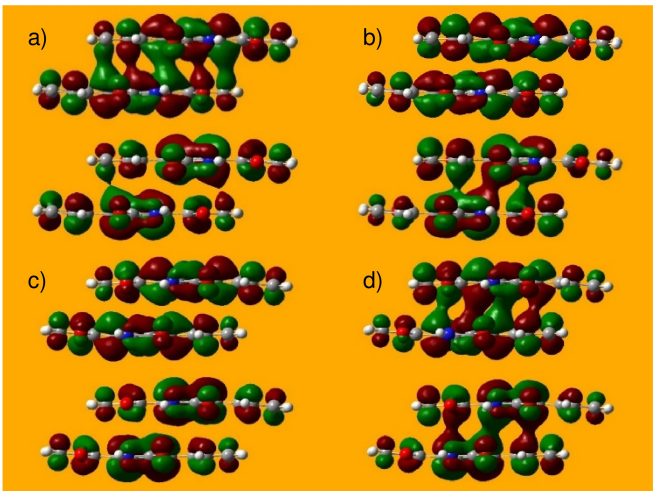

Figure 5. Highest occupied (H, always at the bottom of a given pair) and lowest unoccupied (L, always at the top of a given pair) NTOs for allowed transitions in dimer **3** (a, b) and dimer **4** (c, d) of **FDPP-H** by TD DFT (ωB97X-D/6-31G(d,p)). The second transitions of both dimers are left (a, c), the fourth for dimer **3** (b) and the third for dimer **4** (d) HNTO and LNTO are right. Isovalue is always 0.02, the weights of a hole→particle (HNTO→LNTO) monoexcitation for a given transition are 94.2% (a), 94.9% (b), 88.1% (c) and 88.9% (d).

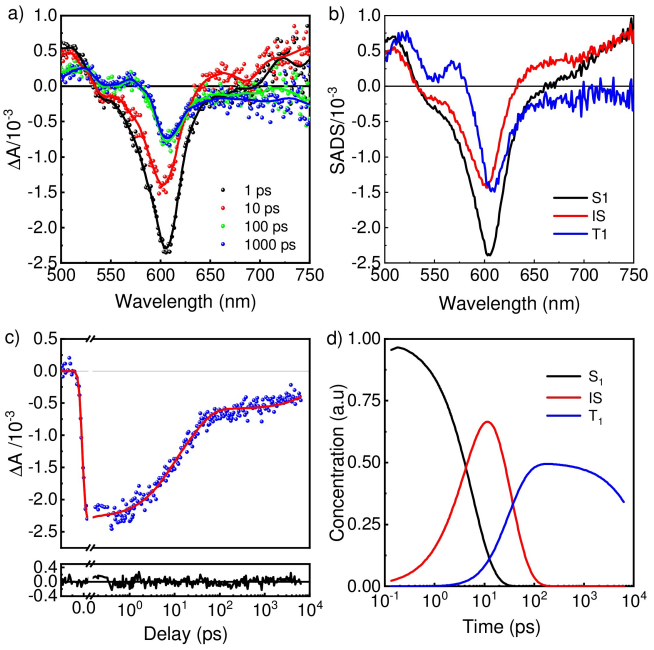

Figure 6. fs-TA spectra of **FDPP-C6** thin film after photoexcitation by laser pulses with central wavelength 450 nm and 200 nJ energy in pulse. (a) Transient absorption spectra at selected time delays shown in the legend. (b) SADS spectra obtained by global analysis. (c) Time course of the difference absorbance (circles) at a selected probe wavelength (600 nm) fitted according to the model in Figure 8 (solid line) (d) Concentration profiles of the target analysis model.

coupling. The difference between absorption and excitation spectra of solid state films (Figure 3) may come from a different character of $2A_u$ state in both arrangements. In **FDPP-EH**, the increment from the pure CT state is missing in the excitation spectrum with respect to the absorption, as it may behave as an excimer-like trap. Excitation to the second allowed state for **FDPP-C6** leads to a localization of the electron density on monomers and, consequently, to its higher participation on overall SSE, coming generally from the lowest allowed state with the partially CT character. Nevertheless, the main portion of photophysical behaviour takes place at the bottom of the first excitonic band (*vide infra*).

The methodology of femtosecond transient absorption (fs-TA) measurements and experimental data analysis are outlined in the experimental section and have been previously described in detail elsewhere.[10d] Similar to most TDPPs studied so far,[10] the singlet fission was observed by fs-TA in both solid-state FDPPs samples. However, notable differences have been found between **FDPP-C6** and **FDPP-EH**.

The differential absorption spectra recorded on thin films in subsequent delay times are shown in Figures 6a and 7a, for **FDPP-C6** and **FDPP-EH**, respectively. The spectra show some common features: the excited state absorption (ESA) bands located at wavelengths longer than 620 nm at early delay times after the excitation and absorption bands located at shorter wavelengths between 450 and 580 nm developed mostly at longer times, assigned to long living triplets. For **FDPP-C6** samples this transition takes place typically within 100 ps. There is also an intermediate ESA band developed within 10 ps after photoexcitation, centered at 600 nm. This band is more pronounced in **FDPP-EH**. Simultaneously to the ESA bands, there is a negative differential absorption observed in the

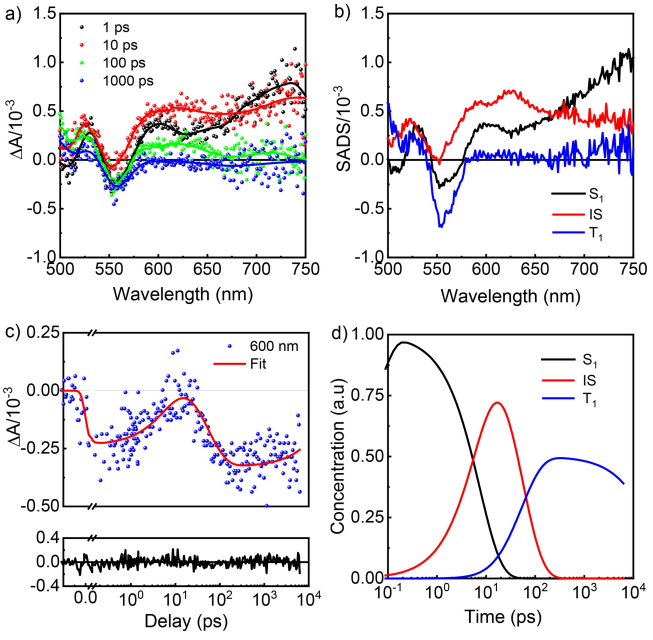

Figure 7. fs-TA spectra of **FDPP-EH** thin film after photoexcitation by laser pulses with central wavelength 450 nm and 200 nJ total energy in pulse. (a) Transient absorption spectra at selected time delays shown in the legend. (b) SADS spectra obtained by global analysis. (c) time course of the difference absorbance (circles) at a selected probe wavelength (555 nm – GSB peak) fitted according to the model in Figure 8 (solid line), (d) Concentration profiles of the target analysis model.

Table 5. Rate constants of excited state decays (k_i from Figure 8) from global analysis of fs-TA data. Φ_T is a triplet state quantum yield.

FDPP	k_1 (ps)	σ (ps)	k_2 (ps)	σ (ps)	k_3 (ps)	σ (ps)	RMS	Φ_T (%)
C6	0.173	0.004	0.018	0.0002	$6.1\cdot10^{-5}$	$2\cdot10^{-6}$	0.000134	160
EH	0.133	0.003	0.0097	0.0001	$4.0\cdot10^{-5}$	$5\cdot10^{-6}$	0.000133	30

wavelength region of the steady-state optical absorption from around 500 to 620 nm, originating in the ground state bleach. The maxima of the ground state bleach are slightly shifted from those observed in the steady state absorption due to the overlap with the positive ESA observed in the same region. No signal that could be ascribed to the stimulated emission has been observed, in agreement with the relatively weak emission of solid state FDPPs derivatives. Analogical fs-TA experiments carried out on dilute solutions of FDPPs in chloroform could not be exactly evaluated due to the considerable photodecomposition of the samples under intense laser excitation (about 200 nJ/pulse). We suppose, that no triplet formation would be detected as in the previous report on **TDPP-C6** and **TDPP-EH**, because of the marginal yield of intersystem crossing (usually <0.01) and the absence of singlet fission[10b] in monomers, in accordance with their high fluorescence quantum yields, even higher for FDPPs as compared to corresponding TDPPs (Table 1). Consequently, solid solutions, more photostable by our experience,[10d] were also not studied.

To explain the time evolution of the measured TA spectra, we performed target analysis testing various three-compartmental models, one fully sequential and the other three that include also a parallel decay channel (Figure S2 and corresponding fitting parameters in Table S2). It has been found that the observed TA spectra of the thin films of the FDPP derivatives under study are best fitted using a three-compartment model (Figure 8), where the initial excited state **1** first relaxes to an intermediate state **2**, from which either decays via singlet fission giving long living triplets or decays nonradiatively through the second parallel branch to the ground state. The corresponding species associated difference spectra (SADS) obtained by the global analysis are shown in Figures 6b and 7b, and the development of the concentrations of the respective components in Figures 6d and 7d for **FDPP-C6** and **FDPP-EH**, respectively. The corresponding rate constants are shown in Table 5. In Figures 6c and 7c, the time course of the TA at the selected wavelength is compared to the TA decay calculated with the parameters obtained from the target analysis, a good agreement between the model and the experimental data. There is a notable difference found in the decay rate constant k_2 of the intermediate state, **FDPP-C6** decays almost twice faster than **FDPP-EH**. Both decay rate constants k_3 for **FDPP-C6** and **FDPP-EH** (Table 5) relate to the triplet state lifetimes in an order of tens of nanoseconds.

The ground state depletion method was used to obtain the triplet-triplet absorption spectra (TTA) and SF quantum yields (Φ_T) of long-lived species assigned to triplets, as previously for TDPPs.[10d] The extracted TTA spectra are shown for both **FDPP-C6** and **FDPP-EH** thin films in Figure 9, and in Figure 10 as decomposed to individual TTA vibronic bands. The SF quantum yields, obtained within this method with a small relative error (10% and 3%) thanks to the relatively well-resolved spectra,

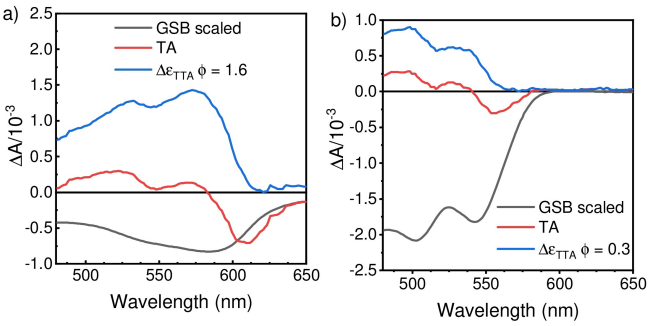

Figure 9. Quantification of the triplet exciton yield in thin films by the singlet depletion method. Triplet-triplet absorption spectrum (blue), scaled GSB at 100% yield (black), and the triplet SADS (red). Left – **FDPP-C6**, right – **FDPP-EH**.

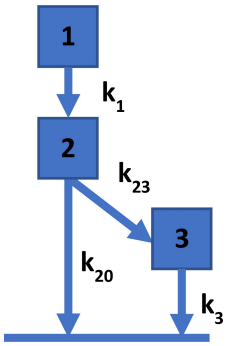

Figure 8. The three-compartmental model used for the target analyses of **FDPP-C6** and **FDPP-EH**.

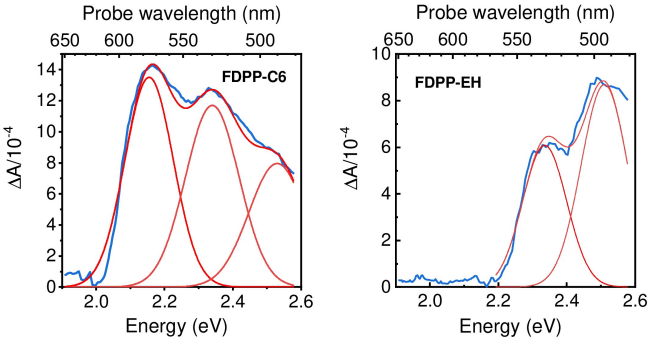

Figure 10. Triplet-triplet absorption spectra of thin films of **FDPP-C6** and **FDPP-EH** with 0–0 maxima at 2.16 eV and 2.34 eV, and $R_{ABS}=0.92$ and 1.44, respectively. Excitation wavelength 450 nm, excitation pulse energy 200 nJ.

were estimated as 160% and 30% for **FDPP-C6** and **FDPP-EH**, respectively. The SF efficiency also determines the branching factor that allows calculating the rate constants k_{23} and k_{20} from the overall decay constant k_2 of the state **2**. The branching ratios $k_{23}:k_{20}$ were 0.80:0.20 and 0.15:0.85 for **FDPP-C6** and **FDPP-EH**, respectively. If considering the net effect, when going from solution to the films, both FDPPs show almost complete aggregation caused quenching (ACQ), as expected for planar stacked chromophores, forming H-type aggregates. But, while fluorescence is almost quantitatively transformed into the triplet formation for **FDPP-C6**, in the case of **FDPP-EH** this process is only minor. We tentatively ascribe the dominant quenching in the latter case to singlet exciton migration[13] to the dark traps, as usual for polycrystallines.[26] Consequently, the formation of correlated triplet pair can be considered a self-trapping process, much more efficient for more tightly bounded **FDPP-C6**.

TTA spectra of FDPPs in Figure 10 show an effect of excitonic coupling, invoked by π-stacked arrangement, on the energy and spectral shape of a monomer's most intense T1→T6 transition (Table S3). These TD DFT computed TTA absorption wavelengths are only slightly blue-shifted with respect to the corresponding TDPPs, thus the experimental FDPPs' TTA spectra generally cover a similar spectral area as those of corresponding TDPPs.[10] The vibrational pattern resembles the shape of the main band in a singlet – singlet SSA (Figure 2, Table 2), only with a bit higher R_{ABS}. The ratios of R_{ABS} (SSA)/R_{ABS} (TTA) are very close (0.73 and 0.76 for **FDPP-C6** and **FDPP-EH**, respectively) suggesting the same effect of excitonic coupling and probably higher (hypothetical) molecular Huang-Rhys factor S for $T_1 \rightarrow T_6$ than for $S_0 \rightarrow S_1$ transition of a monomer. SF is supposed to undergo in the lowest excited singlet state,[1b,7b] i.e. from the bottom of the lowest singlet excitonic band, represented by a forbidden $1A_g$ state for both FDPPs in dimer approximation (Table 3). Supposing, that T_1 energy (and consequently also an energy of correlated triplet pair) is less sensitive to intermolecular effects, due to triplet localization,[27] the changes in $1A_g$ state energy, provoked by π-stacking, may be decisive for SF efficiency. Truly, less efficient **FDPP-EH** has its energy of the lowest singlet state (and thus the driving force for SF) about 0.11 eV lower than **FDPP-C6** (Table 3). Finally, although the prevailing character of the $1A_g$ state of both FDPPs should be FE, the participation of FE/CT mixing is quite clear from NTOs relating to the first forbidden transition, especially for dimer **3**, i.e. **FDPP-C6** (Figure 11). Thus the fast and efficient SF for **FDPP-C6** is conditioned by bigger driving force and pronounced CT mediated delocalization. Nevertheless, LNTO, delocalized between both monomers, enabling accommodation of an arisen triplet pair (biexciton) to both monomers of a dimer, is computed also for dimer **4**, representing **FDPP-EH**, explaining thus its non-zero SF efficiency.

Altogether, the triplet formation through singlet fission in FDPPs is confirmed by the apparent similarity of the triplet species photophysics (fast rise, slow decay and quantum yield over 100% in some cases) and TTA spectral range with broadly verified (including sensitization experiments) TDPPs.[10] Even more conclusive is the analysis of extracted TTA spectra of FDPPs, with the distinct vibronic progressions in solid-state, which show the same effect of excitonic coupling, depending only on the π-stacking geometry, on the shape of corresponding TTA and SSA spectra, i.e. perfectly relating to the theory.[14,17]

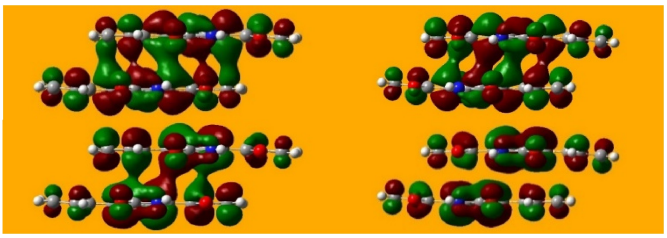

Figure 11. Highest occupied (H, at the bottom of a given pair) and lowest unoccupied (L, at the top of a given pair) NTOs for the first forbidden transitions in dimer **3** (left) and dimer **4** (right) of **FDPP-H** by TD DFT (ωB97X-D/6-31G(d,p)). Isovalue is always 0.02, and the weights of a hole→particle (HNTO→LNTO) monoexcitation for a given transition are 80.7% (left) and 84.7% (right).

Conclusions

Intermolecular interactions considerably affect the physical properties. If the molecules can form crystals with columnar structures fixed by so-called slipped π-stacking, the intermolecular excitonic and electronic coupling between adjacent monomers is decisive for the excited state behavior. Furanyl-substituted diketopyrrolopyrroles were found to form two distinct types of π-stacking, dependent on the branching of their alkyl side chains, as in the case of π-isoelectronic thiophene DPPs. Both these structures were found to form H-aggregates with considerably different energetics in terms of mixed FE and CT states. The different character and strength of both couplings lead to the remarkable diversity in solid-state singlet-singlet (and triplet-triplet) absorption and emission, otherwise similar on the molecular level in solution. Thus, small changes in the molecular structure of these π-isoelectronic compounds enabled tuning the ratio of intensities between 0–1 and 0–0 progressions in solid-state absorption from about 0.68 to 2.84. The combined effect of the molecular structure and solid-state arrangement led to fast and efficient CT mediated singlet fission, with one the highest efficiencies (160%) ever reported within the DPP family and thus potentially perspective for photovoltaics and other applications. The dramatic effect of marginal molecular changes on solid-state photophysics may serve as a guide for the further development of new materials through crystal engineering.

Experimental Section

Syntheses, thin film preparation FDPP, and TDPP pigments were synthesized according to published studies, e.g. in.[28a] *N*,*N*'-dialkylated derivatives **FDPP-C6**, **TDPP-C6**, **FDPP-EH**, **TDPP-EH** were also prepared according to generally known literature approaches.[28b,c]

Solid thin films were deposited onto 2.6×2.6×0.1 cm^3 glass slides, first cleaned in an ultrasonic bath in a clean-room facility (iso class 3) for 10 min in acetone and 10 min in isopropyl alcohol and blow-dried with nitrogen. Physical vapor deposition of 190 ± 10 nm thick films onto substrates tempered at 90 °C was carried out at 1 Å/s deposition rate under $1 \cdot 10^{-6}$ mbar in an MBRAUN MB-ProVap-5 glovebox (< 0.1 ppm H_2O, < 0.1 ppm O_2). The films were subsequently solvent annealed at room pressure and temperature by exposure to saturated dichloromethane vapor. The samples were then kept under vacuum for 24 h to remove the residual solvent.

For the spectroscopic experiments, the thin film samples were encapsulated in a nitrogen atmosphere in a glovebox by enclosing the film in a gap between the substrate and an additional glass window, with poly(ethylene-vinyl acetate) (pEVA) foil inserted between the slides around the perimeter, serving both as a spacer and a gas-tight seal. The whole assembly of supporting glass/pEVA + active layer/cover glass was fixed by binder clips and heated at 90 °C in a vacuum oven for 10 min at $1 \cdot 10^{-2}$ mbar. The samples were cooled to laboratory temperature outside the oven in the glovebox.

Absorption and fluorescence measurements The UV-Vis absorption was measured employing Varian Cary Probe 50 UV-Vis spectrometer (Agilent Technologies Inc.). The steady-state photoluminescence was acquired using SF5 spectrofluorometer (Edinburgh Instruments). The spectra in solution were measured at concentration 2.9×10^{-6} mol/L. The photoluminescence quantum yields (PLQYs) were determined by an absolute method employing integrating sphere SC-30 (Edinburgh Instruments). Photoluminescence of solid-state thin film samples was investigated using Fluorolog 3 (Horiba Jobin Yvon), PLQYs were determined by absolute method using Quanta-Phi integrating sphere. Time-resolved fluorescence was recorded using the time correlated single photon counting method (TCSPC) with a Horiba Jobin Yvon Fluorocube Both R_{ABS} in solid-state spectra[14] and Huang-Rhys factors S in solution were computed from the ratio of the intensities of the first two vibronic progressions I_{0-1}/I_{0-0}.

Transient absorption Femtosecond transient absorption (TA) spectroscopy was performed using HELIOS femtosecond Transient Absorption Spectrometer (Ultrafast Systems, LLC., USA). The experimental setup was described in detail in our previous work.[10d] Unless otherwise noted, the TA experiments were made with the angle $\alpha = 54.7°$ (magic angle) to eliminate the effects of photo-induced anisotropy decay on the recorded kinetics. This approach allowed using a polarization filter in the probe light collection optics located in between the sample and the photodetector, which reduced the artifacts caused by stray light from the pump beam. Thin films of the FDPP derivatives were excited with laser pulses with the central wavelength $\lambda_{ex} = 450$ nm. Energy per pulse was typically around 200 nJ/pulse with the beam crosssection around 300 μm FWHM. The sample was mounted on the translation stage and it was moving with a scan rate of 1 mm/s during the measurement. The samples were measured in the air under ambient conditions.

Quantum chemical calculations Final geometries of centrosymmetric cofacial slipped stacked dimers were obtained using DFT with M06-2X[29] xc functional with 6-311G(d,p) basis set by full geometrical optimization, starting from various centrosymmetric geometries. No symmetrical constraints were used. The geometries were checked by vibrational analysis. Binding energies were computed as the difference between dimer energy, obtained with the same functionals using an extended 6-311 + G(2d,p) basis sets with involved counterpoise (CP) procedure,[30] and optimized monomer energy, obtained in the same way. The geometries used for TD DFT calculations were obtained from dimer optimization with ωB97X-D functional[31] and 6-31G(d,p) basis set. All calculations were carried out with Gaussian 09 software.[32] The resulting geometries were characterized by plane-to-plane (PP) and center-to-center (CC) distances between DPP cores of both monomers in a dimer.[17] Computed PP and CC were evaluated by Mercury 3.9.[33] Excitation energies of the lowest six singlet states of the dimers were computed by TD DFT with ωB97X-D xc functional and 6-31 + G(d,p) basis set. Natural transition orbitals (NTO) were calculated by TD DFT with ωB97X-D xc functional and 6-31G(d,p) basis set. Triplet-triplet absorption of the monomers was modelled by TD DFT B3LYP (6-311 + G(2d,p)) excitation energies on T_1 geometry (DFT B3LYP (6-311G(d,p)).

Supporting Information

The authors have cited additional references within the Supporting Information.[34]

Acknowledgements

The authors thank the Czech Science Foundation grant No. 19-22783S for the financial support. Computational resources were supplied by the project "e-Infrastruktura CZ" (e-INFRA CZ LM2018140) supported by the Ministry of Education, Youth, and Sports of the Czech Republic. M. A. T., D. R., and J. P. thanks the Czech Science Foundation grant No. 22-02005S for support of the TA spectroscopy part.

Conflict of Interests

The authors declare no conflict of interest.

Data Availability Statement

The data that support the findings of this study are available in the supplementary material of this article.

Keywords: singlet fission · diketopyrrolopyrrole · solid state photophysics · triplet excitons · aggregates

[1] a) M. B. Smith, J. Michl, *Chem. Rev.* **2010**, *110*, 6891–6936; b) D. Casanova, *Chem. Rev.* **2018**, *118*, 7164–7207; c) K. Miyata, F. S. Conrad-Burton, F. L. Geyer, X.-Y. Zhu, *Chem. Rev.* **2019**, *119*, 4261–4292.
[2] a) J. Xia, S. N. Sanders, W. Cheng, J. Z. Low, J. Liu, L. M. Campos, T. Sun, *Adv. Mater.* **2017**, *29*, 1601652; b) T. Wang, B. Y. Zhang, H. L. Zhang, *Macromol. Rapid Commun.* **2022**, *43*, 2200326; c) A. J. Baldacchino, M. I. Collins, M. P. Nielsen, T. W. Schmidt, D. R. McCamey, M. J. Y. Tayebjee, *Chem. Rev.* **2022**, *3*, 021304; d) A. J. Carrod, V. Gray, K. Börjesson, *Energy Environ. Sci.* **2022**, *15*, 4982–5016.
[3] X. Qiao, D. Ma, *Mater. Sci. Eng. R* **2020**, *139*, 100519.
[4] a) R. Casillas, I. Papadopoulos, T. Ullrich, D. Thiel, A. Kunzmann, D. M. Guldi, *Energy Environ. Sci.* **2020**, *13*, 2741–2804; b) T. Ullrich, D. Munz, D. M. Guldi, *Chem. Soc. Rev.* **2021**, *50*, 3485–3518.
[5] a) L. Wang, Y. Olivier, O. V. Prezhdo, D. Beljonne, *J. Phys. Chem. Lett.* **2014**, *5*, 3345–3353; b) Z. Havlas, J. Michl, *Isr. J. Chem.* **2016**, *56*, 96–106;

c) E. A. Buchanan, J. Michl, *J. Am. Chem. Soc.* **2017**, *139*, 15572–15575; d) K. M. Felter, F. C. Grozema, *J. Phys. Chem. Lett.* **2019**, *10*, 7208–7214.
[6] a) N. V. Korovina, N. F. Pompetti, J. C. Johnson, *J. Chem. Phys.* **2020**, *152*, 040904; b) T. Hasobe, S. Nakamura, N. V. Tkachenko, Y. Kobori, *ACS Energy Lett.* **2021**, *7*, 390–400; c) S. Paul, V. Karunakaran, *J. Phys. Chem. B* **2022**, *126*, 1054–1062; d) Y. Hong, M. Rudolf, M. Kim, J. Kim, T. Schembri, A. M. Krause, K. Shoyama, D. Bialas, M. I. S. Röhr, T. Joo, H. Kim, D. Kim, F. Würthner, *Nat. Commun.* **2022**, *13*, 4488.
[7] a) K. Bhattacharyya, A. Datta, *J. Phys. Chem. C* **2017**, *121*, 1412–1420; b) M. H. Feng, A. I. Krylov, *J. Phys. Chem. C* **2018**, *122*, 25753–25763; c) N. A. Pace, B. K. Rugg, C. H. Chang, O. G. Reid, K. J. Thorley, S. Parkin, J. E. Anthony, J. C. Johnson, *Chem. Sci.* **2020**, *11*, 7226–7238; d) G. Mayonado, K. V. Vogt, J. D. B. Van Schenck, L. Zhu, G. Fregoso, J. Anthony, O. Ostroverkhova, M. W. Graham, *J. Phys. Chem. C* **2022**, *126*, 4433–4445.
[8] I. Papadopoulos, M. J. Álvaro-Martins, D. Molina, P. M. McCosker, P. A. Keller, T. Clark, A. Sastre-Santos, D. M. Guldi, *Adv. Energy Mater.* **2020**, *10*, 20011496.
[9] a) T. Mukhopadhyay, A. J. Musser, B. Puttaraju, J. Dhar, R. H. Friend, S. Patil, *J. Phys. Chem. Lett.* **2017**, *8*, 984–981; b) C. M. Mauck, Y. J. Bae, M. Chen, N. Powers-Riggs, Y.-L. Wu, M. R. Wasielewski, *ChemPhotoChem* **2018**, *2*, 223–233; c) S. J. Bradley, M. Chi, J. M. White, C. R. Hall, L. Goerigk, T. A. Smith, K. P. Ghiggino, *Phys. Chem. Chem. Phys.* **2021**, *23*, 9357–9364.
[10] a) P. E. Hartnett, E. A. Margulies, C. M. Mauck, C. E. Miller, Y. Wu, Y. L. Wu, T. J. Marks, M. R. Wasielewski, *J. Phys. Chem. B* **2016**, *120*, 1357–1366; b) C. M. Mauck, P. E. Hartnett, E. A. Margulies, L. Ma, C. E. Miller, G. C. Schatz, T. J. Marks, M. R. Wasielewski, *J. Am. Chem. Soc.* **2016**, *138*, 11749–11761; c) C. M. Mauck, P. E. Hartnett, Y. L. Wu, C. E. Miller, T. J. Marks, M. R. Wasielewski, . *Chem. Mater.* **2017**, *29*, 6810–6817; d) D. Rais, P. Toman, J. Pfleger, U. Acharya, Y. R. Panthi, M. Menšik, A. Zhigunov, M. A. Thottappali, M. Vala, A. Marková, S. Střitesky, M. Weiter, M. Cigánek, J. Krajčovič, K. Pauk, A. Imramovský, A. Zaykov, J. Michl, *ChemPlusChem* **2020**, *85*, 2689–2703; e) A. M. Levine, G. He, G. Bu, P. Ramos, F. Wu, A. Soliman, J. Serrano, D. Pietraru, C. Chan, J. D. Batteas, M. Kowalczyk, S. J. Jang, B. L. Nannenga, M. Y. Sfeir, E. H. R. Tsai, A. B. Braunschweig, *J. Phys. Chem. C* **2021**, *125*, 12207–12213; f) N. Maity, W. Kim, N. A. Panjwani, A. Kundu, K. Majumder, P. Kasetty, D. Mishra, R. Bittl, J. Nagesh, J. Dasgupta, A. J. Musser, S. Patil, *Nat. Commun.* **2022**, *13*, 5244; g) J. Zhou, H. Liu, S. Liu, P. Su, W. Wang, Z. Li, Z. Liu, Y. Chen, Y. Dong, X. Li, *J. Phys. Chem. B* **2022**, *126*, 6483–6492.
[11] L. Shen, Z. Tang, X. Wang, H. Liu, Y. Chen, X. Li, *Phys. Chem. Chem. Phys.* **2018**, *20*, 22997–23006.
[12] A. B. Pun, L. M. Campos, D. N. Congreve, *J. Am. Chem. Soc.* **2019**, *141*, 3777–3781.
[13] O. P. Dimitriev, *Chem. Rev.* **2022**, *122*, 8487–8593.
[14] a) F. C. Spano, *Acc. Chem. Res.* **2010**, *43*, 429–439; b) N. J. Hestand, F. C. Spano, *Acc. Chem. Res.* **2017**, *50*, 341–350; c) N. J. Hestand, F. C. Spano, *Chem. Rev.* **2018**, *118*, 7069–7163; d) C. Zheng, C. Zhong, C. J. Collison, F. C. Spano, *J. Phys. Chem. C* **2019**, *123*, 3203–3215.
[15] R. M. Young, M. R. Wasielewski, *Acc. Chem. Res.* **2020**, *53*, 1957–1968.
[16] a) H. Zang, Y. Zhao, W. Z. Liang, *J. Phys. Chem. Lett.* **2017**, *8*, 5105–5112; b) L. Wang, L. Lin, J. Yang, Y. Wu, H. Wang, J. Zhu, J. Yao, H. Fu, *J. Am. Chem. Soc.* **2020**, *142*, 10235–10239; c) L. Wang, W. Cai, J. Sun, Y. Wu, B. Zhang, X. Tian, S. Guo, W. Z. Liang, H. Fu, J. Yao, *J. Phys. Chem. Lett.* **2021**, *12*, 12276–12282.
[17] S. Luňák Jr., M. Weiter, M. Vala, *ChemPhysChem* **2022**, *23*, e202200252.
[18] M. Kirkus, L. Wang, S. Mothy, D. Beljonne, J. Cornil, R. A. J. Janssen, S. C. J. Meskers, *J. Phys. Chem. A* **2012**, *116*, 7927–7936.
[19] C. Fu, F. Bélanger-Gariépy, D. F. Perepichka, *CrystEngComm* **2016**, *18*, 4285–4289.
[20] M. A. Naik, N. Venkatramaiah, C. Kanimozhi, S. Patil, *J. Phys. Chem. C* **2012**, *116*, 26128–26137.
[21] J. Gierschner, H. G. Mack, L. Lüer, D. Oelkrug, *J. Chem. Phys.* **2002**, *116*, 8596–8609.
[22] A. Oleson, T. Zhu, I. S. Dunn, D. Bialas, Y. Bai, W. Zhang, M. Dai, D. R. Reichman, R. Tempelar, L. Huang, F. C. Spano, *J. Phys. Chem. C* **2019**, *123*, 20567–20548.
[23] M. Kratochvíl, M. Ciganek, Ci. Yumusak, H. Seelajaroen, I. Cisařová, J. Fábry, M. Vala, S. Luňák, M. Weiter, N. S. Sariciftci, J. Krajcovic, *Dyes Pigm.* **2022**, *197*, 109884.
[24] a) K. Pauk, S. Luňák Jr., A. Růžička, A. Marková, A. Mausová, M. Kratochvíl, K. Melánová, M. Weiter, A. Imramovský, M. Vala, *Chem. Eur. J.* **2020**, *26*, 4341–4348; b) K. Pauk, S. Luňák Jr., A. Růžička, A. Marková, K. Teichmanová, A. Mausová, M. Kratochvíl, R. Smolka, T. Mikysek, M. Weiter, A. Imramovský, M. Vala, *RSC Adv.* **2022**, *12*, 34797–34807.
[25] S. Canola, G. Bagnara, Y. Dai, G. Ricci, A. Calzolari, F. Negri, *J. Chem. Phys.* **2021**, *154*, 124101.
[26] J. Gierschner, J. Shi, B. Milián-Medina, D. Roca-Sanjuán, S. Varghese, S. Y. Park, *Adv. Opt. Mater.* **2021**, *9*, 2002251.
[27] M. Zubiria-Ulacia, J. M. Maxtain, D. Casanova, *Phys. Chem. Chem. Phys.* **2020**, *22*, 15908–15918.
[28] a) M. Grzybowski, E. Glodkowska-Mrowka, V. Hugues, W. Brutkowski, M. Blanchard-Desce, D. T. Gryko, *Chem. Eur. J.* **2015**, *21*, 9101–9110; b) P. Data, A. Kurowska, S. Pluczyk, P. Zassowski, P. Pander, R. Jedrysiak, M. Czwartosz, L. Otulakowski, J. Suwinski, M. Lapkowski, A. P. Monkman, *J. Phys. Chem. C.* **2016**, *120*, 2070–2078; c) E. Ripaud, D. Demeter, T. Rousseau, E. Boucard-Cétol, M. Allain, R. Po, P. Leriche, J. Roncali, *Dyes Pigm.* **2012**, *95*, 126–133.
[29] Y. Zhao, D. G. Truhlar, *Theor. Chem. Acc.* **2008**, *120*, 215–241.
[30] S. F. Boys, F. Bernardi, *Mol. Phys.* **2002**, *100*, 65–73.
[31] J. D. Chai, M. Head-Gordon, *Phys. Chem. Chem. Phys.* **2008**, *10*, 6615–6620.
[32] Gaussian 09 (Revision **D.01**), M. J. Frisch, W. G. Trucks, H. B. Schlegel, G. E. Scuseria, M. A. Robb, J. R. Cheeseman, G. Scalmani, V. Barone, B. G. Mennucci, A. Petersson, H. Nakatsuji, M. Caricato, X. Li, H. P. Hratchian, A. F. Izmaylov, J. Bloino, G. Zheng, J. L. Sonnenberg, M. Hada, M. Ehara, K. Toyota, R. Fukuda, J. Hasegawa, M. Ishida, T. Nakajima, Y. Honda, O. Kitao, H. Nakai, T. Vreven, J. A. Montgomery Jr., J. E. Peralta, F. Ogliaro, M. Bearpark, J. J. Heyd, E. Brothers, K. N. Kudin, V. N. Staroverov, R. Kobayashi, J. Normand, K. Raghavachari, A. Rendell, J. C. Burant, S. S. Iyengar, J. Tomasi, M. Cossi, N. Rega, J. M. Millam, M. Klene, J. E. Knox, J. B. Cross, V. Bakken, C. Adamo, J. Jaramillo, R. Gomperts, R. E. Stratmann, O. Yazyev, A. J. Austin, R. Cammi, C. Pomelli, J. W. Ochterski, R. L. Martin, K. Morokuma, V. G. Zakrzewski, G. A. Voth, P. Salvador, J. J. Dannenberg, S. Dapprich, A. D. Daniels, Ö. Farkas, J. B. Foresman, J. V. Ortiz, J. Cioslowski, D. J. Fox. C. T. Wallingford, Gaussian, Inc. **2009**.
[33] C. F. Macrae, P. R. Edgington, P. McCabe, E. Pidcock, G. P. Shields, R. Taylor, M. Towler, J. van de Streek, *J. Appl. Crystallogr.* **2006**, *39*, 453–457.
[34] X. Y. Shen, Y. J. Wang, H. Zhang, A. Qin, J. Z. Sun, B.Z Tang, *Chem. Commun.* **2014**, *50*, 8747–8750.

Manuscript received: August 30, 2023
Revised manuscript received: September 13, 2023
Accepted manuscript online: September 19, 2023
Version of record online: October 12, 2023

RESEARCH ARTICLE

Furanyl-substituted diketopyrrolopyrroles (DPP) with different branching of the alkyl side chains were studied. Both formed two distinct types of π-stacking leading to H-aggregates with considerably different energetics in terms of mixed lowest Frenkel and charge transfer (CT) states. The combined effect of the molecular structure and solid-state arrangement lead to fast and efficient CT mediated singlet fission, with one of the highest efficiencies (160%) ever reported within the DPP family.

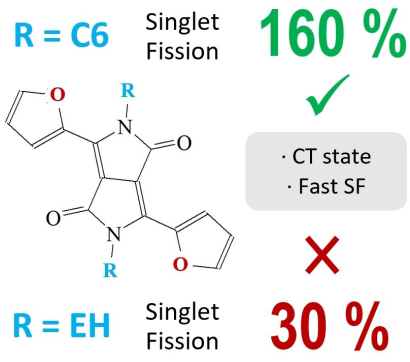

Dr. M. Kratochvíl, M. A. Thottappali, Dr. S. Luňák, Jr., Dr. K. Pauk, Dr. D. Rais, A. Marková, Dr. J. Pfleger, Prof. A. Imramovský, Prof. M. Vala**

1 – 10

Solid-State Absorption, Luminescence, and Singlet Fission of Furanyl-Substituted Diketopyrrolopyrroles with Different π-Stacking Arrangements